Advanced Powder Technology 34 (2023) 104136

Contents lists available at ScienceDirect

Advanced Powder Technology

journal homepage: www.elsevier.com/locate/apt

Original Research Paper

Solid-fluid mixing behavior of conical spouted beds with internal devices

A. Atxutegi [a,*], P. Kieckhefen [b], S. Pietsch-Braune [b], R. Aguado [a], J. Bilbao [a], S. Heinrich [b], M. Olazar [a]

[a] Dept. of Chemical Engineering, University of the Basque Country (UPV/EHU), PO Box 644 – E48080 Bilbao, Spain
[b] Institute of Solids Process Engineering and Particle Technology, Hamburg University of Technology (TUHH), Denickestrasse 15, 21073 Hamburg, Germany

ARTICLE INFO

Article history:
Received 2 February 2022
Received in revised form 20 April 2023
Accepted 14 June 2023
Available online 24 June 2023

Keywords:
Gas-solid mixing
RTD
Particle cycle time
CFD-DEM simulation

ABSTRACT

The effect of draft tubes and fountain confiner on the gas and solids mixing behavior is studied in conical spouted beds. Accordingly, the bed porosity has been determined in different hydrodynamic regimes of 1.1, 1.25 and 1.5 u/u_{ms}, with beds equipped with draft tubes of 0%, 56% and 100% opening ratio. These devices significantly affect the gas residence time and particle cycle time distributions, which are further improved by using a fountain confiner, specially when high inlet gas flow rates are desired. The addition of this device was found to remove stagnant gas pockets over the annular zone, while reducing the particle cycle time by 15% with the *OSDT* configuration at 1.5 u/u_{ms}. This reduction heavily depends on the distance between the bed surface and the fountain confiner. By including draft tubes, the expected particle cycle time can be more than doubled due to the reduced annular-spot solids circulation. Therefore, it was found that a combination of internal devices and operating flow rate present a promising strategy to control the gas flow pattern, while keeping the distribution of particles cycle times required for each application.

1. Introduction

Mixing is a highly relevant issue in gas–solid contact systems due to the influence of turbulence and phase interactions on the bed performance, and therefore on the properties of the final product. Although fluidized beds are a well for contacting gas and solid phases, spouted beds are increasingly used for the treatment of particles that are difficult to handle in a conventional reactor, as is the case of coarse particles and those with highly irregular shape, wide size distribution and/or cohesive nature. The study of these contactors involves certain complexities due to the heterogeneous structure in the bed, comprising distinctive regions: as are a central spout, a fountain and an annular zone, Fig. 1. These regions vary in size and shape depending on the operating conditions and the presence of internal devices, such as draft tubes [1,2]. The latter are specifically used to increase the operational range and spouting stability. Furthermore the knowledge about the size and features of each region, most applications (either physical or chemical) rely on the information about the flow patterns of the gas and solid phases in order to properly design a system that is tailored to the process requirements. For example, milliseconds are required for fast or ultrafast pyrolysis [3,4], a few seconds for cracking reactions [5] and longer reaction times for combustion or gasification [6,7].

The gas flow pattern is generally characterized by the study of the residence time distribution (*RTD*) [8], from which the degree of mixing and gas pockets can be identified. *RTD* curves have been obtained in spouted beds for a few configurations and gas flow rates [9,10], and they are the evidence of a poor understanding of the effect that operating conditions, internal devices and particle shape have on the fluid pattern in the bed. Nevertheless, this information is essential for the application of this technology in both chemical and physical processes. Concerning the solid phase, given that spouted beds have generally been used in batch mode in lab scale reactors, the cycle time is used to characterize the overall bed circulation [11]. This information is of great relevance in both batch and continuous operation in order to predict heat and mass transfer homogeneity of the gas–solid contact in the bed, and is of uttermost significance in certain processes, such as coating and granulation. Studies have been conducted in conical spouted beds to obtain this information in certain configurations, but, given the number of data points required for a significant statistical inference, it has only been obtained for hydrodynamic conditions close to the minimum spouting velocity [12]. Particle tracking in the fountain through the transparent wall is difficult due to the high sampling frequency required and the difficulties to identify the

* Corresponding author.
E-mail address: aitor.achutegui@tuhh.de (A. Atxutegi).

https://doi.org/10.1016/j.apt.2023.104136

Nomenclature

α	Void fraction field, -	D_o	Inlet diameter, m
$\mathbf{u}$	Fluid velocity, $m\,s^{-1}$	γ	Contactor angle, ^{o}
θ	Transported scalar, -	ω_H	Leg width, m
μ	Molecular viscosity, $Pa\,s$	ω_T	Draft tube operture ratio, -
ρ	Density, $kg\,m^{-3}$	L_H	Draft tube entrainment height, m
C	Tracer concentration, $mol\,m^{-3}$	Ar	Archimedes number, -
$F(t)$	Cumulative residence time distribution function, -	t_c	Particle cycle time, s
$E(t)$	Residence time distribution function, -	H_C	Conical section height, m
t	Time, s	H_i	Measuring height, m
Θ	Dimensionless time, -	D_i	Contactor base diameter, m
V_r	Contactor volume, m^3	D_o	Contactor inlet diameter, m
Q_i	Volumentric flow rate, $m^3\,s^{-1}$	D_T	Draft tube diameter, m
t_c	Particle cycle time, s	L_T	Draft tube length, m
H_o	Static bed height, m		

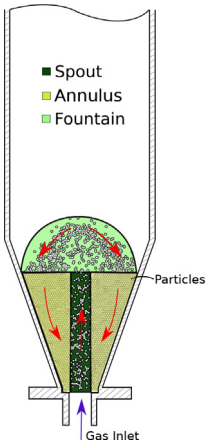

Fig. 1. Description of the different spouted bed regions, with color coded annular, spout and fountain zones.

traced particle. However, most real systems do not operate in this hydrodynamic regime, as it provides a low solid circulation flow rate, and therefore a high risk of clogging and collapsing the spout.

Computer simulations, and especially *CFD-DEM* modeling, have enabled the simulation of spouted beds of various contactor [13] geometries and configurations [14] by tracking every single particle in the domain [15,16]. The overall draft tube effect in spouted bed circulation has already been studied by other researchers [17,15]. However, the use of a purely spherical solid description becomes really limited, taking into account that in most industrial scale applications non-spherical particles are employed. Thus, other authors [18,19] and this group [20] have striven to simulate no-spherical particles through the superquadric description described by

$$\left(\left\|\frac{x}{r_x}\right\|^{n_2}+\left\|\frac{y}{r_y}\right\|^{n_2}\right)^{n_1/n_2}+\left\|\frac{z}{r_z}\right\|^{n_1}=1 \tag{1}$$

where x, y and z describe a given point in local coordinates,n_1 and n_2 are the blockiness values and r_x, r_y and r_z are the shape parameters in each dimension, respectively. This description was first described by [21] and has been subsequently implemented in *LIGGGHTS* [22] and other simulation tools. Liu et al. [23] described the effect of particle shape in the overall time averaged velocity behaviour with a clear analysis of in increase fountain instability as the particle aspect ratio is increased. Wang et al. [19] and Gao et al. [18] also performed spouting simulations of irregular particles by using the superquadric approach with a focus in the solid velocity profiles, particle mixing index and particle orientation. Mahmoodi et al. [24] performed *CFD-DEM* simulations of fine sand, assuming spherical particle, with the use of draft tubes. Feng et al. [25] and Wang et al. [26] focused on the simulation of spouted fluidized-bed and the relative particle mixing times where analyzed for a number of flow-rates along with particle velocity and pressure drop fluctuations under different inlet gas velocities. However, most of these studies are focused on short time simulations where the solid velocity field is left to stabilize and the local velocity values are compared against velocimetry [27] or tomographic [28] data. Thus, these simulations are not run for long times in order to infer the influence of parameters such as particle shape, size and the addition of new devices such as draft tubes and fountain confiners, on the overall solid residence time. The residence times of both, solid and gas, phases in spouted bed are a critical factor for the reactor control and design. Questions such as the minimum distance between confiner and surface bed or the expected increased residence time of the gas phase arise when trying to include a new device. This work aims to answer these questions by running *CFD-DEM* simulations through relatively long times in order to infer the influence of process parameters, particle shape and internal devices on the solid and gas residence time distribution in conical spouted beds.

2. Materials and procedure

The experimental equipment has been extensively described in previous publications [29,30], and so a brief outline of the configurations is provided here. The geometric parameters of the conical spouted bed, Fig. 2, are as follows: upper cylindrical diameter, D_C, of 36 cm, contactor angle, γ, of 36°, conical section height, H_C, of 45 cm, base diameter, D_i, of 6.2 cm and inlet diameter, D_o, of 5 cm.

Two draft tube types have been used in the simulations, i.e., the solid draft tube (*SDT*) and the open-sided draft tube (*OSDT*), Fig. 2b, in order to study the effect of the opening ratio on the gaseous phase residence times and packing properties. The *OSDT* has a length, L_T, of 22 cm, a tube diameter, D_T, of 5.5 cm and an opening ratio, ω_T, of 56%, whereas the *SDT* has the same length and diameter but an entrainment height, L_H, of 7.5 cm. Thus, the configuration without draft tube (*WDT*) is in fact a fully opened draft tube ($\omega_T = 1$), whereas the *SDT* corresponds to a fully closed tube ($\omega_T = 0$). Simulations have been run for each configuration, with glass beads of 2 mm and 4 mm in diameter, and lentils and pellets of 3.4 mm and 1.2 mm in equivalent volume diameter, respectively. For each configuration and material, the effect of all these

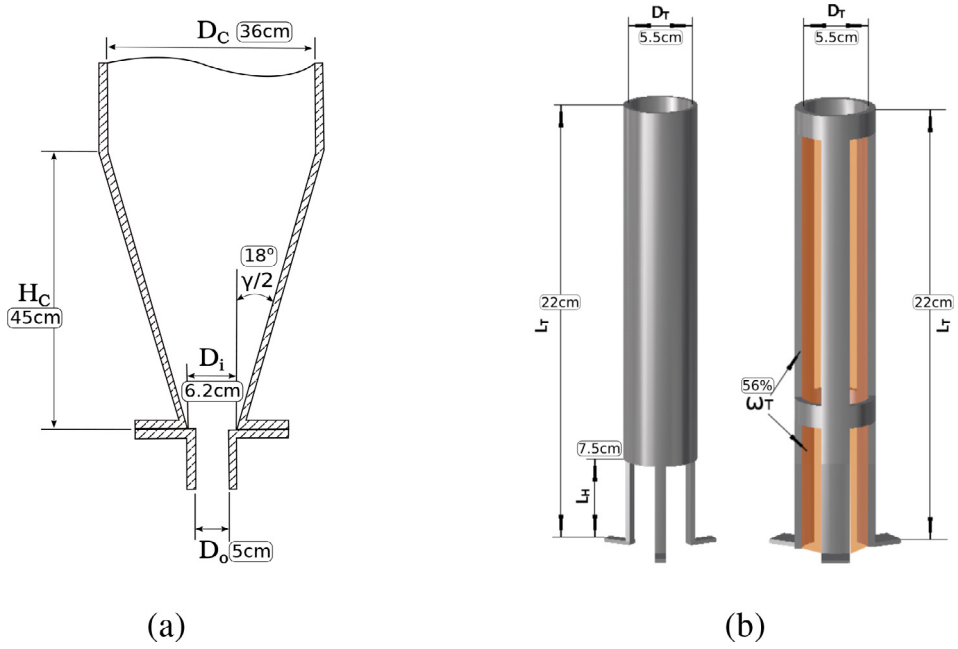

Fig. 2. Main parameters of (a) the contactor and (b) the solid draft tube (left) and open-sided draft tube (right).

parameters on the hydrodynamic regime has been studied by running simulations at 1.1, 1.25 and 1.5 times the minimum spouting velocity (1.1 u_{ms}, 1.25 u_{ms} and 1.5 u_{ms}).

2.1. CFD-DEM simulation of superquadric particles

The simulation of the spouted bed was accomplished by using a custom branch of the *CFDEMCoupling* which provides for a good interface to couple OpenFOAM (*CFD*) for the simulation of the fluid phase and *LIGGGHTS* for the simulation of the discrete phase (*DEM*). Given the open source nature of the code, it allows for custom modifications depending on the requirements of the user. In this case, the code was modified in order to allow for a range of drag models for irregular materials, the implementation and validation of which, where deeply explained in a previous work [20]. As a summary, the internal solid velocity field was experimentally obtained through particle tracking velocimetry (*PTV*) and compared against *CFD-DEM* simulations of superquadrics with different materials and under varying hydrodynamic conditions. Superquadric representation following Eq. 1 allowed for the simulation of a wide range of particle shapes under a single implementation. Table A.1 shows the main governing equation of *CFD-DEM*, while Table B.3 in the Appendix show the main simulation parameters that where chosen for these simulations. From previous studies the Sanjeevi et al. [31] drag model was selected as the best suited to represent the gas–solid momentum exchange while a divided void fraction model was selected for the simulation of the correct void fraction field and subsequent exchange terms, as otherwise clipped void fraction values or unreasonably high drag values are calculated [20]. Particle volume (V_P) to *CFD* cell volume (V_C) was kept around 3 (Appendix Table B.2) in order to run the $CFD-DEM$ in an unresolved manner. For those regions where the *CFD* cell is required to be of smaller, a satellite point approach similar to that of [18,19] was used in order to divide the particle volume among the neighboring cells. This implementation and explanation can be found in the already mentioned previous work, resulting in a smoother void fraction field.

2.2. Simulation of the gas residence time

The gas residence time is characterized by conducting a step tracer injection to a passive scalar, θ, at the inlet of the contactor, which is transported through the simulation domain as follows:

$$\frac{\partial \theta}{\partial t} + \nabla \cdot (\mathbf{u}\theta) - \nabla^2 \left(\frac{\mu_f}{\rho_f} \theta \right) = 0 \tag{2}$$

where μ_f and ρ_f are the effective fluid viscosity and fluid density, respectively. This passive scalar needs to be transported in a realistic fluid simulation, which has been performed using the κ-ωSST turbulence model [32] for given inlet flow rates. Once the step injection has been done, the tracer concentration has been tracked at the outlet in order to obtain cumulative residence time distribution (F curve), as well as the residence time distribution (E curve), as follows:

$$F(t) = \frac{C(t)}{C_0} = \int_0^t E(t)dt \tag{3}$$

Considering that each combination of configuration and solid type has a given minimum spouting velocity, u_{ms}, the mixing degrees have been compared at the hydrodynamic regimes of 1.1, 1.25 and 1.5 u_{ms} to ascertain the influence of flow rate on the *RTD* curves. In order to compare curves corresponding to different time scales, a dimensionless residence time, Θ, has been defined:

$$\Theta = \frac{tV_r}{Q_i} \tag{4}$$

where t is the time after injection, V_r is the contactor volume and Q_i is the inlet volume flow rate. This way, the effect of different inlet flow rates is removed and an effective comparison of the overall gas dispersion can be done.

2.3. Simulation of the solid cycle time

The particle cycle time is defined as the time each particle takes to travel through the three bed zones, i.e, spout, annulus, and fountain. When experimental measurements are conducted, the cycle

time is assumed to be the time that a particle stays in the annular zone [33], as this is the region, where particles stay most of the time (lowest velocity). Nevertheless, the simulations do not involve this limitation, as every particle is tracked in each time step. Thus, the cycle time may account for the time spent by the particle to cross the three zones; that is, the time spent by the particle leaving the spout through the upper side of the draft tube, $H_i = 24$ cm, to return again to this position. In order to get a representative simulation of the cycle times, once stable spouting has been reached, it has been maintained for 2*s*, and the simulation has been then run until every particle in the domain has completed at least two cycles. This way, the solid cycle time distribution gets stabilized and average, maximum, and minimum cycle times can be inferred for each configuration and flow rate. It should be noted that, each time the flow rate is changed in a given configuration, all the cycle times are reset and another 2*s* are provided for the new hydrodynamic regime to settle and stabilize the system.

3. Results

The gas–solid mixing is first described based on the void fraction profiles and the influence of particle shape and internal devices on these profiles. Then, an analysis of the gas phase residence time distribution and solid cycle times is performed to design a spouted bed with the required operational features.

3.1. Void fraction

In multiphase reactors, such as conical spouted beds, the mixing between phases is generally characterized by the void fraction field, which, in turn, is heavily affected by the internal devices. To analyze this effect, Fig. 3 shows the void fraction profiles along the spout axis obtained for each configuration and flow rate. As expected, the void fraction along the axis sharply decreases in a stretch from the bed inlet to a certain location in the spout. This applies for all configurations and flow rates analyzed, and is a consequence of solid cross-flow from the annulus into the spout. Moreover, the type of internal device is highly influential regardless of the flow rate.

When no internal device is used (*WDT* configuration), Fig. 3a, the void fraction values are lower than in the other configurations studied, suggesting a more packed spout due to particle freely flow from the annulus into the spout. An increase in the flow rate increases the dilution of the spout and also the resulting fountain height. When an open-sided draft tube is used (*OSDT* configuration), Fig. 3b, the minimum void fraction is attained at lower location in the spout axis. Furthermore, this inverse peak is lower as the flow-rates is increased due to particle dilution. When analyzing the cross-section view shown in Fig. 3b for the height of $H_i = 22$ cm, the void fraction field is significantly affected by the presence of draft tube wall and opened areas, with a lower void fraction closer to the wall as solid circulation is neglected and higher void fractions in the open areas in a characteristic star pattern already mentioned in the literature [27]. The solid draft tube, Fig. 3c, leads a characteristic void fraction field with the minimum value located just below the entrainment height ($L_H = 7.5$ cm) and a reasonably steady value inside the draft tube ($7.5 < H_i < 22$cm), which is consequence of the undisturbed particles in the spout, as they are protected by a fully closed draft tube.

The use of irregular particles requires the implementation of a divided void fraction model for superquadric particles [34] and this feature results in more oscillatory void fraction fields, Fig. 4, for all configuration and particle shapes.

A comparison of Fig. 4a with Fig. 3a shows that the void fraction profile along the axial direction is less influenced by the flow rate when irregular particles are spouted. This feature is consistent

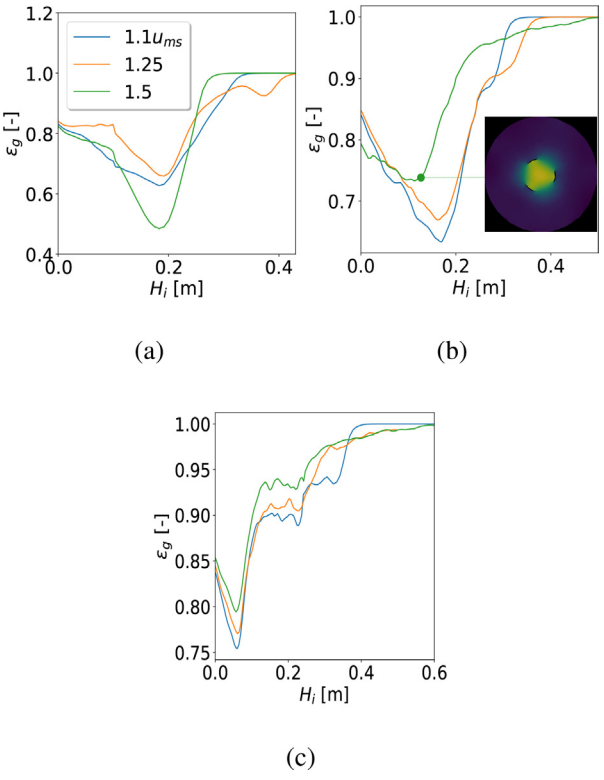

Fig. 3. Void fraction profiles along the spout axis for $\bar{d}_p$=4 mm glass beads at different flow rates in (a) *WDT*, (b) *OSDT* and (c) *SDT* configurations; (b) radial void fraction view at a given cross-sectional cut in the *OSDT* configuration.

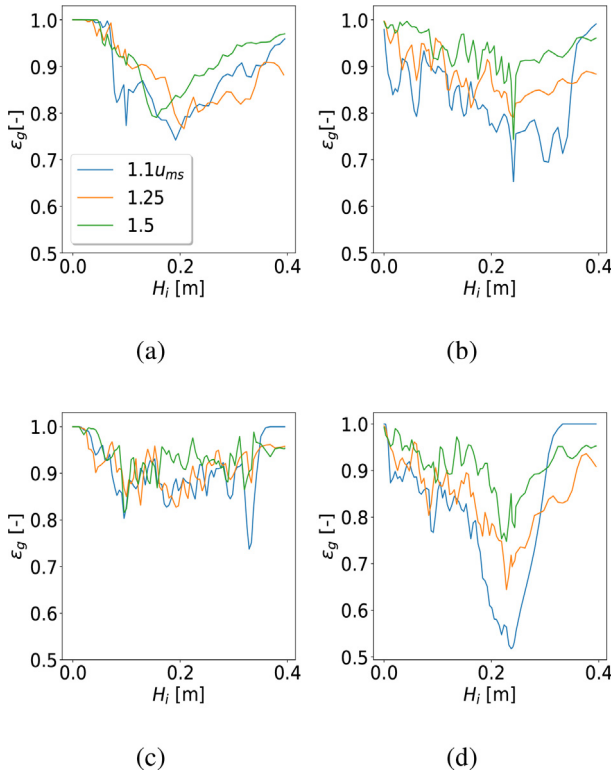

Fig. 4. Void fraction profiles along the contactor axis at the three spouting velocities for beds of lentils in (a) *WDT*, (b) *OSDT* and (c) *SDT* configurations, and (d) for beds of pellets in the *OSDT* configuration.

with the fact that irregular particles do not roll, and hence the opening of the spout from the static bed is much more abrupt than with spherical particles. Thus, an increase in the flow rate does not significantly affect the overall solid packing, as each grain tends to be intertwined with its neighbors. Overall, the *WDT* configuration leads to a progressive decrease in the void fraction, as particles are incorporated into the spout at any bed level. Once the bed surface is reached, $H_o = 22$ cm, the void fraction along the fountain axis increases due to particle diversion in this zone. When internal devices are used, Figs. 4, the solid incorporation is limited according to the opening ratio of the draft tube. Thus, there is a less pronounced decrease when the *OSDT* configuration is used than when the *WDT* configuration is used, whereas only a sharp decrease in the void fraction along the entrainment height, $L_H = 7.5$ cm, is observed for the *SDT* configuration. The latter is explained by the fact that the entrainment zone in the *SDT* configuration is the only spout section, where particles may incorporate into the spout. All these trends apply to ellipsoidal particles (lentils), but cylindrical pellets in the *OSDT* configuration lead to clearly different trends. Thus, Fig. 4d shows that these beds attain much lower void fraction values at all flow rates, and therefore particle assemblies are more densely packed, which may significantly affect the gas–solid mixing and mass transfer rates in any physical or chemical processes. However, as the flow rate is increased, the axial profile resembles those in Fig. 4b for lentils in the *OSDT* configuration.

3.2. Gas residence time distribution

The gas residence time in spouted beds has already been studied by other authors, who noted a very short residence time in the spout, which is influenced by the configuration and flow rates used [35]. Therefore, this study deals with the *RTD* in conical spouted beds in order to determine the most suitable mixing pattern for a given application and detect inefficiencies in the gas flow distribution. Based on the dimensionless residence time, Θ, it is possible to compare the *RTD* curves obtained under different flow rates and configurations. Each simulation is run for 5 Θ in order to let the gas phase flow through the reactor completely.

Fig. 5 shows the evolution of *RTD* curves when spherical particles are spouted in beds of different configurations and at each flow rate. When the *WDT* configuration is used with $\bar{d}_p$ = 4 mm glass beads, Fig. 5a, *E* and *F* curves undergo significant changes when the flow rate is increased from 1.1 u_{ms} to 1.5 u_{ms}, with the latter leading to a significantly longer tail, even though the mean residence time, $\bar{t}_g$, is slightly shorter than for the lower rates of 1.1 u_{ms} and 1.25 u_{ms}, which is evidence of a fluid element population corresponding to gas back mixing. When the same configuration is used with glass beads of $\bar{d}_p$ = 2 mm, Fig. 5b, this second population is also present at 1.5 u_{ms}, albeit the tail in the *E* curve is shorter. In view of Fig. 5, the type of configuration has great influence on the gas flow pattern in the reactor. Thus, a comparison of Fig. 5c with Fig. 5a clearly shows that the *OSDT* configuration creates significantly longer tails, which is evidence of more backflow and dead zones. At the highest flow rate analyzed of 1.5 u_{ms}, the *F* curve does not reach the inlet concentration of 1 at the outlet, even for the longest residence time considered (5 Θ). This behavior gets more pronounced when using the *SDT* configuration, Fig. 5d, with none of the flow rates reaching the inlet concentration. In fact, the outlet concentration is lower as the flow rate is increased. This configuration allows attaining a very short average residence time ($\bar{t}_g$), which is explained by a big fraction of the gas phase bypassing most of the reactor volume, i.e., it mainly goes through the spout zone. It seems that an increase in the flow rate together with internal devices create high shear forces in the spout zone, which hinders radial dispersion of the air flow. Furthermore, the

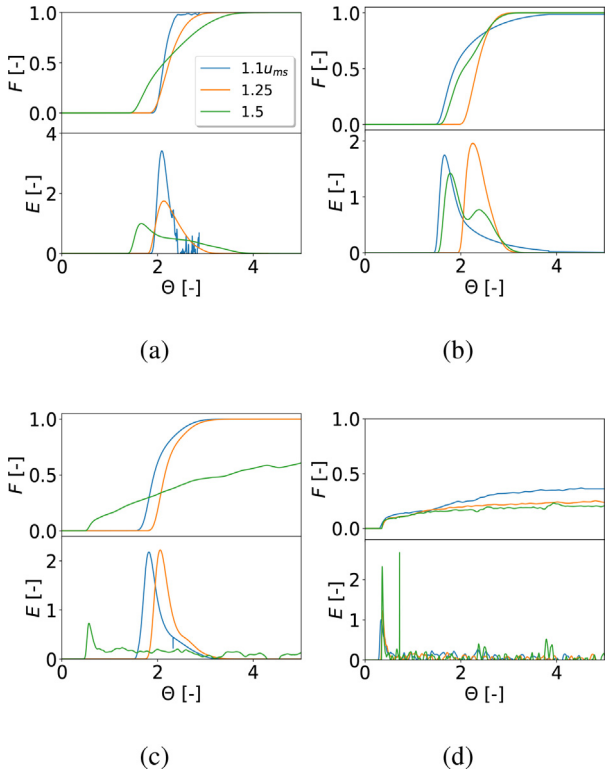

Fig. 5. *RTD* evolution in the *WDT* configuration with (a) $\bar{d}_p$=4 mm and (b) $\bar{d}_p$=2 mm glass beads, and in (c) *OSDT* and (d) *SDT* configurations with $\bar{d}_p$=4 mm glass beads, in a conical spouted bed at different flow rates.

tracer leaving the annulus on the upper surface of the bed is diluted by the flow that has bypassed the bed through the spout, which results in long times for the withdrawal of the tracer from the contactor.

Fig. 6 shows that beds of irregular particles, specifically lentils, behave similarly to those of regular ones. Thus, the *WDT* configuration, Fig. 6a, leads to a reasonable radial gas diversion (a final value of 1 in the *F* curves), which is not the case when internal devices are used, either open-sided (*OSDT* configuration), Fig. 6b, or solid tubes (*SDT* configuration), Fig. 6c. The latter configuration provides the shortest residence time for any inlet flow rate, as most of the gas is driven through the center of the spouted bed without having the chance to radially divert, as is the case in the *OSDT* configuration.

Therefore, in these cases, in which the gas phase cannot radially divert, a fraction of the reactor volume is underused, which leads to low process efficiency and inefficient use of the energy supplied to the system [36,37]. As an example of this poor radial diversion, Fig. 7 shows the distribution of the tracer in the contactor at a given time for a configuration with the open-sided draft tube. In order to avoid this undesirable effect, the insertion of a fountain confiner [38] is proposed, as it is a passive mixing device that may contribute to correcting this problem without a significant increase in cost or system complexity.

3.2.1. Fountain confiner as a gas mixing device

It is well known that the use of a fountain confiner above the bed surface, Fig. 8b, modifies the flow pattern of the solid phase from that corresponding to a free fountain, such as the one in Fig. 8a, a, to one that does not oscillate or leads to the formation of a crater, as happens with irregular particles.

This device not only changes the solid flow pattern, but it also modifies the gas flow distribution. Thus, a comparison of Fig. 6b,

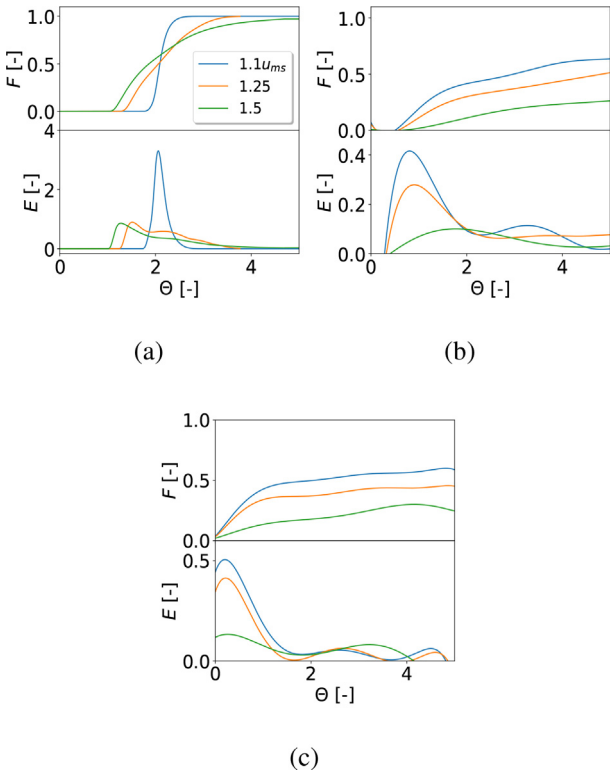

Fig. 6. Evolution of *E* and *F* curves for the gas in (a) *WDT*, (b) *OSDT* and (c) *SDT* configurations with lentils in a conical spouted bed at varying flow rates.

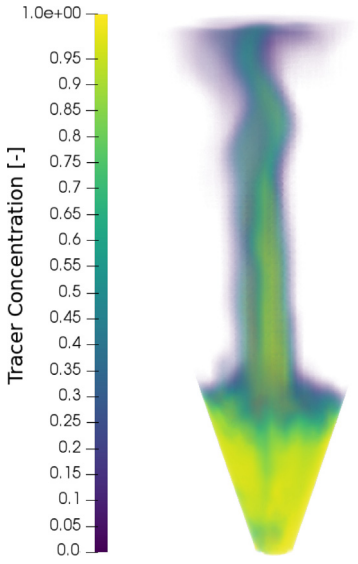

Fig. 7. Tracer distribution in the *OSDT* configuration at 1.5u_{ms} showing the presence of gas dead zones, especially around the fountain core above the bed surface.

corresponding to the previous configuration without confiner, with Fig. 9 for the system with confiner, shows that the tracer concentration at the outlet stream reaches that of the inlet in a reasonable time, for the three inlet flow rates analyzed. Furthermore, the *E* curves are closer to a plug flow regime than in the absence of confiner, with a flow pattern that is hardly affected by the flow rate, which is a highly desirable fact given the use of the flow rate as an actuation parameter in control loops [39].

However, the use of such device is likely to have a significant effect on the particle cycle time, which is a key parameter when

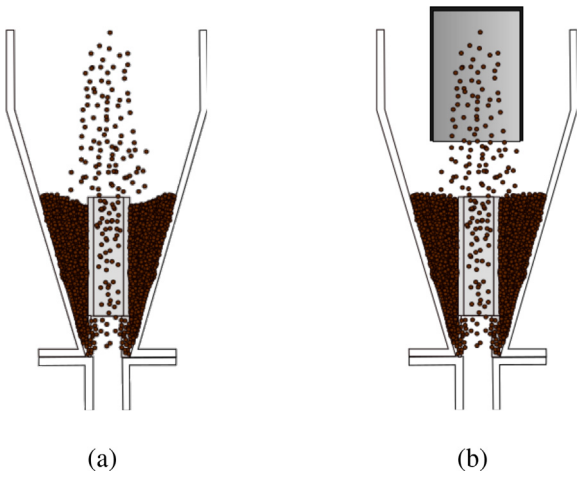

Fig. 8. Upper surface of the bed (a) without confiner and (b) with confiner.

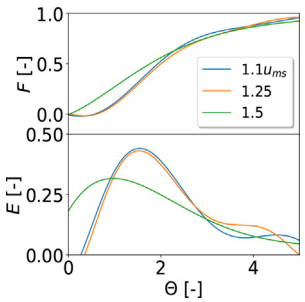

Fig. 9. *F* and *E* curves for the *OSDT* configuration with fountain confiner at various flow rates.

the solid is the material of interest. Accordingly, attention must be paid to all these effects on the solid phase.

3.3. Solid phase cycle times

Many operations in the spouted beds, such as drying, coating and granulation, involve the use of the solid phase in batch mode. Thus, the solid phase is contained within the contactor for the whole duration of the process, and there is therefore no residence time distribution [11]. Nevertheless, the solid phase performance is characterized through the solid cycle time, which is defined as the time particles take to travel through the three regions in the bed, i. e, annulus, spout and fountain [40]. This parameter determines the solid circulation rate and, in the case the catalyst undergoes deactivation, the cycles a particle may complete before it is replaced. In addition to the average cycle time, the maximum and minimum cycle times provide information, as they are related to the cycles completed along the contactor wall and those close to the surface of the bed, respectively [41]. Given the significance of these parameters, a number of correlations have been proposed [40,12] to predict the average cycle time in conical spouted beds of different configurations. For a *WDT* configuration, the following correlation has been proposed:

$$\bar{t_c} = 33.51 Ar^{-0.12} \left(\frac{H_0}{D_0}\right)^{0.13} tan(\gamma)^{0.78} \quad (5)$$

where *Ar* is the Archimedes dimensionless number, H_o is the static bed height, D_O is the inlet diameter and γ is the contactor angle. Eq. 5 describes the cycle time for only the *WDT* configuration, as the addition of any internal device requires the inclusion of

dimensionless modules accounting for their geometry, i.e., the aperture ratio, ω_H, for the *OSDT* and the entrainment height, L_H, for the *SDT* configurations. The correlations corresponding to these configurations are as follows:

$$\bar{t_c} = 101.82Ar^{-0.18}\left(\frac{H_O}{D_O}\right)^{0.48}\left(\frac{\omega_H}{D_O}\right)^{0.31}tan(\gamma)^{0.87} \quad (6)$$

$$\bar{t_c} = 4.08Ar^{-0.06}\left(\frac{H_O}{D_O}\right)^{1.71}\left(\frac{L_H}{D_O}\right)^{-0.79}tan(\gamma)^{0.94} \quad (7)$$

Fig. 10a compares the average solid cycle times obtained with the simulations and those with the correlations in the literature for the configurations analyzed. As observed, the results obtained by both procedures are consistent for both particle sizes ($\bar{d_p}$ = 2 mm and $\bar{d_p}$ = 4 mm glass beads). The highest deviation is obtained for the *SDT* configuration with a maximum deviation of 12%. It should be noted that, even though the current system corresponds to the geometry for which the cycle time correlations where obtained [40], the design of the solid draft tube has been slightly changed, with the narrower legs in the current design being partially responsible for a lower cycle time estimation. One of the main constrains of these correlations is that they are limited to a regime close to the minimum spouting velocity. Nevertheless, the current model allows exploring the evolution of the average particle cycle time at higher flow rates, Fig. 10b.

Cycle time studies are usually limited to a hydrodynamic regime close to the minimum spouting velocity due to the high number of reliable data points required (in the order of hundreds) for a clear definition of the cycle time distribution and the fact that it becomes increasingly complicated to visually measure particle cycle times as the circulation rate increases. Nevertheless, this information together with the gas flow distribution is crucial to ascertain the efficiency of the gas–solid contact and even to design the best locations for feeding the solid into the bed. Thus, taking advantage of the fact that numerical simulations do are not restrained in terms of flow-rate or particle occlusion the particle cycle time distributions have been determined by simulation for each configuration, Fig. 11. As observed, there is a clear influence of the type of internal device used on the distribution of cycle times, albeit their average cycle time being similar.

When the *WDT* configuration is used, Fig. 11a, there is a small fraction of particles describing very short cycles (below 1 s), i.e., they do not descend along the wall, but complete the cycle in a zone around the spout on the bed surface, and therefore by-pass most of the annular zone. Nevertheless, the vast majority of the

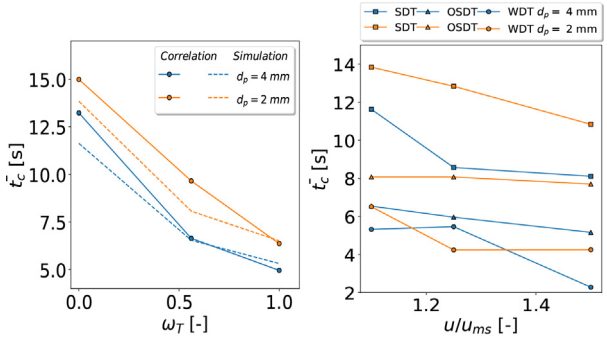

(a) (b)

Fig. 10. Comparison of (a) simulated cycle times with those obtained using the correlations by Estiati et al. [12] and (b) the evolution of the average cycle time with flow rate predicte.d by simulation.

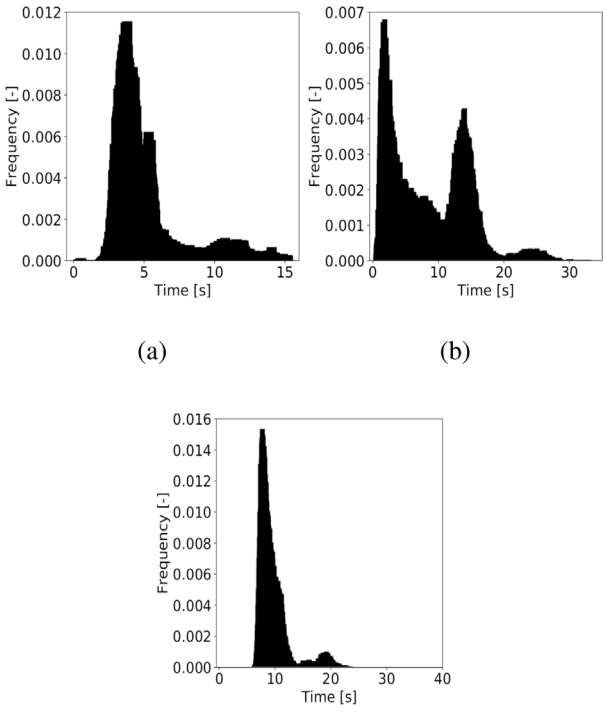

(a) (b) (c)

Fig. 11. Cycle time distributions at $1.1u_{ms}$ with $4mm$ glass beads for the configurations of (a) *WDT*, (b) *OSDT* and (c) *SDT*.

particles have a skewed cycle distribution corresponding to the bulk of the annular zone. Finally, there is a considerable fraction completing long cycles (above 10 s in Fig. 11a) corresponding to the particles descending along the wall to the bottom. They have the longest cycle times due to particle–wall friction along with the longer distance they have to travel in the bed. In the case of the *OSDT* configuration, Fig. 12b, the population with long cycles along the wall is also evident. However, the main bulk of particles is distributed into two main populations, which is evidence of two preferential zones in which there is solid cross-flow from the annulus into the spout through the apertures of the draft tube. The distribution with the longer cycle times corresponds to the preferential solid cross-flow in the lower section of the draft tube and the one with the shorter cycles in the upper section. It is noteworthy that, although the draft tube is partially opened, the non-opened fraction of the tube in the *OSDT* configuration leads to longer cycles than in the absence of draft tube (*WDT* configuration). Furthermore, a lower minimum spouting velocity is required when an open-sided draft tube is used, which leads to lower turbulence, and therefore to increasing cycle times. When a solid draft tube is used (*SDT* configuration), Fig. 11c, the particle cycle time distribution has a similar shape as the one shown in Fig. 11a for the *WDT* configuration, but in this case the distribution is shifted towards higher cycle times, as all particles require a minimum time to travel from the top of the bed to the entrainment region. Fig. 12 shows the distributions for beds of lentils operated at the three flow rates analyzed in the three configurations studied.

As observed in Fig. 12a, corresponding to lentils operated in the *WDT* configuration at 1.1 u_{ms}, spouting of irregular particles leads to a cycle time distribution skewed to long cycle times. As the flow rate is increased, the cycle time distribution shifts towards shorter cycles. However, moderate and high flow rates still show a significant tail due to the friction with the wall. In the *OSDT* configuration, the tail corresponding to the slowest particles along the

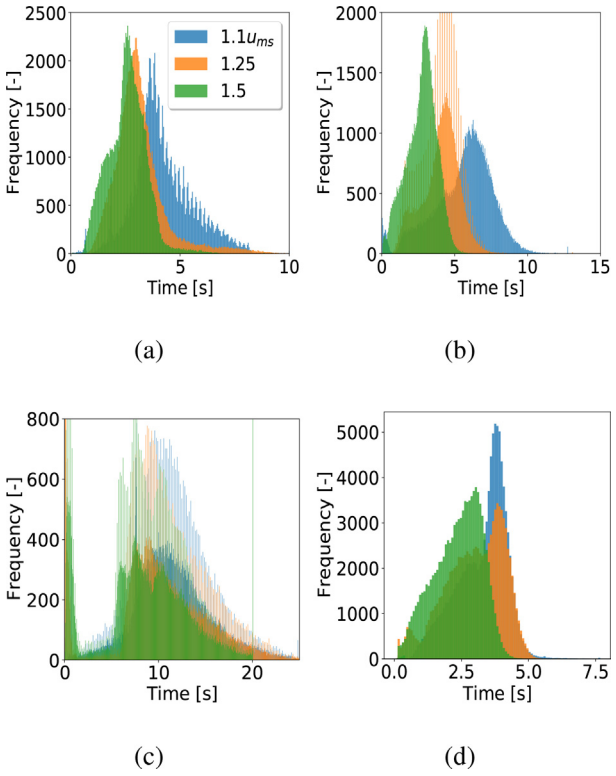

Fig. 12. Solid cycle time distributions under different flow rates for lentils used in the configurations (a) *WDT*, (b) *OSDT*, (c) *SDT*, and (d) pellets in the *OSDT* configuration.

wall is evident for the lowest flow rate. Nevertheless, as the flow rate is increased, the cycle times are shorter and there is hardly any tail corresponding to the wall particles, which is consequence of the higher solid circulation. The *SDT* configuration is the one with the smallest change in the cycle time distribution with flow rate. The cycle time is hardly reduced by increasing the air flow rate, which is explained by the low solid circulation when a solid draft tube used (independently of the flow rate), as well as the low minimum spouting velocity required with this type of tube. These facts lead to a marginal decrease in the cycle time with considerable increase in air flow rate. When *ABS* pellets are spouted instead of lentils in a *OSDT* configuration, Fig. 12b, the more compact packing of these particles leads to a decrease in the cycle times at all flow rates. Nevertheless, there is hardly any difference between those corresponding to 1.1u_{ms} and 1.25u_{ms}, and they are lower when the flow rate is increased to 1.50u_{ms}, which is evidence that turbulence is not attained with these types of particles until moderate flow rates (1.50u_{ms}) are used.

Based on the results mentioned, particle cycle time is affected by both solid properties and internal devices. Thus, the fountain confiner (*FC*), which is commonly used for either correcting spout oscillations or improving gas distribution, has a significant effect on the particle cycle time. In order to study the effect the confiner has on the spouted bed dynamics, a bed-to-confiner distance, H_f, of 0.07 cm has been taken, which was reported by Tellabide et al. [42] as the optimum for bed stabilization, and also for allowing the air stream to get into the confiner and leave it through this gap (no confiner pressurization neither slugging bed). The confiner used in this simulation is of 15 cm in diameter, and has been inserted in the conical spouted bed together with an open-sided draft tube, i.e., the *OSDT* configuration has been used, Fig. 13a.

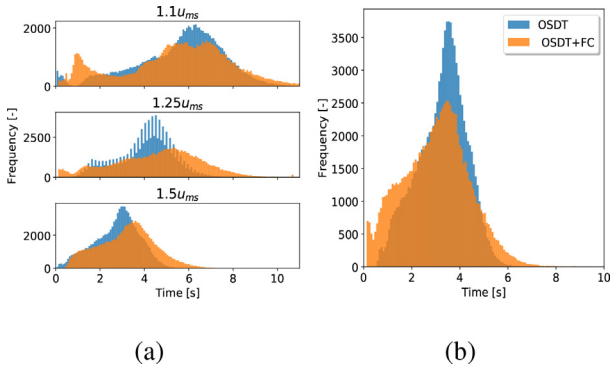

Fig. 13. Effect of the confiner on the solid cycle time in a conical spouted bed equipped with an *OSDT*, operating (a) at various flow rates with a confiner-to-bed distance of H_f = 7 cm and (b) at 1.5u_{ms} with a confiner-to-bed distance of H_f = 14 cm.

As expected, when low flow rates are used (1.1u_{ms}), the solid cycle time is shortened with the addition of the fountain confiner (*FC*). Furthermore, the use of this device also creates a new solid population with short cycles (< 2 s), as particles coming from the confiner are directly fed into the inner zone on the annulus surface. When the flow rate is increased to 1.25u_{ms}, although the distribution is slightly wider with the confiner, there is hardly any difference in the average cycle time with and without confiner. Finally, when the highest flow rate is used (1.5u_{ms}), the average cycle time increases slightly with the presence of the fountain confiner. This is explained by the higher horizontal component of the gas velocity in the gap between the confiner and the bed surface (H_f), which in this case is 7 cm. This radial gas velocity at the top of the bed makes a significant amount of particles coming down from the confiner to be thrown against the contactor wall, thus balancing the shortening effect the fountain confiner has on the particle cycle time. In case this effect is not desired, it may be avoided by rising the fountain confiner, i.e., increasing H_f. Thus, Fig. 13b shows the effect of placing the confiner at H_f = 14 cm on the cycle time. As observed, high flow rates do not have any influence on the cycle time when the confiner is placed sufficiently high. This is due to the increased cross sectional area available for the air to leave the confiner, resulting in lower horizontal components of gas and solid velocities, which would otherwise drag some particles in the horizontal direction in the fountain section between the confiner and the bed surface.

4. Conclusions

CFD-DEM simulations have been run for various draft tube configurations, solid types and flow rates. The distribution of void fraction undergoes significant changes when a draft tube is used. Thus, the configuration without draft tube (*WDT*) leads to a decrease in bed voidage as the bed level in the spout is higher, which is explained by the solid cross-flow from the annulus into the spout at every location in the spout-annulus interface. The use of an internal device smoothens the decrease in bed voidage, as it reduces the solid transfer from the annulus into the spout.

The residence time of the gas is greatly influenced by the internal device and the flow rate for both regular and irregular particle beds. Thus, a high excess in flow rate and/or close draft tube do not allow for radial diversion of the gas phase, resulting in gas bypassing most of the reactor volume, which must be avoided in order to increase the gas–solid contact in the bed and make use of the whole contactor volume. To that end, the use of a fountain

confiner has proven to avoid gas by-passing, by forcing the radial diversion of the air leaving the spout, as well a better homogenization of the gas flow.

Internal devices influence the solid cycle time. The presence of a draft tube moves the cycle time distribution towards higher times, whereas the shape of the distribution is affected by the flow rate and the use of a fountain confiner. Furthermore, the latter shortens the average particle cycle time, with this shortening being heavily affected by the bed-to-confiner distance. Therefore, the residence time of the gas and the cycle time of the particles may be controlled by acting on the gas flow rate and bed-to-confiner distance.

Declaration of Competing Interest

The authors declare that they have no known competing financial interests or personal relationships that could have appeared to influence the work reported in this paper.

Acknowledgments

This work has been carried out with the financial support from the Spain's Ministries of Economy and Competitiveness (*CTQ*2016-75535-*R*(*AEI*/*FEDER*, *UE*)) and Science and Innovation (*PDI*2019-107357*RB-I*00(*AEI*/*FEDER*, *UE*)), the Basque Government (*IT*218-19) and the University of the Basque Country UPV/EHU (*US*16/21). Aitor Atxutegi is grateful for his Ph.D. grant from the University of the Basque Country UPV/EHU(*PFI*15-2017).

Appendix A. Governing equations

The *CFD-DEM* coupling is attained by connecting *LIGGGHTS* for the simulation of *DEM* and OpenFOAM ($v.8$) for the modeling of the fluid field by using *CFDEM-Coupling*. In Table A.1 a summary of the main governing equation for *CFD-DEM* are given. The solver is a custom adaptation of the standard *cfdemSolverPiso* in order to be able to handle superquadric particles including the corresponding drag and torque force already outlined in a previous work [20].

In order to communicate the required information between *CFD* and *DEM* fields the communication scheme *Few2Few* outlined in [43] has been used in order to reduce the inter-processor communication and only exchange data of neighboring processors, increasing simulation performance and reducing memory requirements.

Appendix B. Domain meshing and simulation setting

The current study is conducted through unresolved *CFD-DEM*. Thus, the cell size needs to be bigger than the particle size. The general rule of thumb is to target a V_C/V_p of 3 for the whole domain. However, in some regions where small opening or sharp

Table A.1
Governing equations of *CFD-DEM* simulations.

CFD	
continuity equation	$\frac{\partial \alpha_f \rho_f}{\partial t} + \nabla \cdot (\alpha_f \rho_f \mathbf{u_f}) = \mathbf{0}$
momentum equation	$\frac{\alpha_f \rho_f \mathbf{u_f}}{\partial t} + \nabla \cdot (\alpha_f \rho_f \mathbf{u_f} \mathbf{u_f}) = -\alpha_\mathbf{f} \triangle \mathbf{p} - \mathbf{K_{sf}}(\mathbf{u_f} - \mathbf{u_s}) + \nabla \cdot (\alpha_f \tau) + \alpha_\mathbf{f} \rho_\mathbf{f} \mathbf{g} + \mathbf{f}$
exchange term	$\mathbf{K_{sf}} = \frac{\alpha_f \lvert \sum \lvert \mathbf{F_d} \rvert}{\mathbf{V_C} \lvert \mathbf{u_f} - \mathbf{u_s} \rvert}$
DEM	
linear momentum	$m \frac{d\mathbf{u_s}}{dt} = m\mathbf{g} + \mathbf{f_{s,s}} + \mathbf{f_{s,w}} + \mathbf{f_{s,f}}$
angular momentum	$I_i \frac{d\omega_i}{dt} + \omega_\mathbf{i} \times \mathbf{I_i} \omega_\mathbf{i} = \tau_\mathbf{i}$
normal force	$\mathbf{f_n} = -(\mathbf{k_n} \delta_\mathbf{n} \mathbf{n_{i,j}} - \gamma_\mathbf{n} \mathbf{u_{n,i,j}})$
tangential force	$\mathbf{f_t} = \begin{cases} -k_{t,i,j} \delta_t t_{i,j} - \gamma_t \mathbf{u_{t,i,j}} & \lvert \mathbf{f_{ct,i,j}} \rvert \leqslant \mu_s \lvert \mathbf{f_{cn,i,j}} \rvert \\ -\mu_s \lvert \mathbf{f_{cn,i,j}} \rvert \mathbf{t_{i,j}} & \lvert \mathbf{f_{ct,i,j}} \rvert > \mu_s \lvert \mathbf{f_{cn,i,j}} \rvert \end{cases}$
CFD − *DEM* Coupling	
Drag coefficient	$C_{D,\lambda} = C_{D,\lambda=0^o} + (C_{D,\lambda=90^o} - C_{D,\lambda=0^o}) sin^2 \lambda$
Drag force	$F_D = \frac{1}{8} C_D \pi \rho_f d_p^2 \epsilon_g^2 \lvert \mathbf{u_f} - \mathbf{v_s} \rvert (\mathbf{u_f} - \mathbf{v_s}) \epsilon_\mathbf{g}^{-\chi}$
Tangential coefficient	$C_{T,\lambda} = \left(\frac{c_1}{Re'^2_2} + \frac{c_2}{Re'^4_4}\right) sin\lambda^{\left(1+c_5 Re'^6_6\right)} cos\lambda^{\left(1+c_7 Re'^8_8\right)}$
Tangential force	$\mathbf{F_T} = \frac{1}{16} \pi \mathbf{C_T} \rho_\mathbf{f} \lvert \mathbf{u_r} \rvert^2 \mathbf{d_{eq}^3}$
Tangential force direction	$\mathbf{T} = \lvert \mathbf{F_T} \rvert \frac{(\mathbf{u_r} \cdot \mathbf{e_o})}{\lVert \mathbf{u_r} \cdot \mathbf{e_o} \rVert} \frac{(\mathbf{u_r} \times \mathbf{e_o})}{\lVert \mathbf{u_r} \times \mathbf{e_o} \rVert}$

Table B.2
Mesh size comparison for the different configurations in the conical spouted bed.

Configuration	Material	Cell Number	V_C/V_p		
			Min	Mean	Max
WDT	Glass 4 *mm*	74018	0.77	3.06	4.72
OSDT		75627	0.84	2.85	4.87
SDT		77956	0.49	2.94	4.98
WDT	Glass 2 *mm*	530581	0.65	3.42	4.87
OSDT		556270	0.45	3.13	5.17
SDT		601023	0.41	3.73	4.97
WDT	Pellet	74154	1.31	4.09	7.56
OSDT		79042	1.25	4.52	7.73
SDT		81147	1.04	4.36	7.8
WDT	Lentil	74018	0.91	3.52	5.57
OSDT		77922	0.97	3.36	5.75
SDT		79042	0.58	3.24	5.52

Table B.3
DEM input frictional parameters for each material.

Parameter	Glass Beads		Lentils	Pellets
$d_{p,eq}$ [mm]	4.0	2.0	3.72	3.12
ρ_p [kg/m^3]	2500	2500	850	1120
E [Pa]	$7.5^{.8}$	$7.5^{.8}$	$3^{.8}$	$4^{.6}$
Δt_{DEM} [s]	$1 \cdot 10^{-5}$	$2 \cdot 10^{-6}$	$5.1 \cdot 10^{-6}$	$2.5 \cdot 10^{-6}$
Δt_{CFD} [s]	$2 \cdot 10^{-3}$	$2 \cdot 10^{-3}$	$2 \cdot 10^{-3}$	$2 \cdot 10^{-3}$
Number of particles	55875	430100	100329	200317
Geldart type	D	D	D	D
Restitution coefficient, $\kappa_{p,p}$ [-]	0.98	0.94	0.91	0.9
Restitution coefficient, $\kappa_{p,w}$ [-]	0.85	0.95	0.95	0.92
Frictional coefficient, $\gamma_{p,p}$ [-]	0.185	0.17	0.31	0.36
Frictional coefficient, $\gamma_{p,w}$ [-]	0.45	0.45	0.4	0.45
Rolling friction, $\mu_{r_{p,p}}$ [-]	0.1	0.07	0.05	0.06
Rolling friction, $\mu_{r_{p,w}}$ [-]	0.1	0.07	0.1	0.1
Rolling damping coefficient, $\gamma_{r,f}$ [-]	0.15	0.15	0.1	0.1

turns of the container wall are present it is not possible to use big *CFD* cells while keeping a good quality mesh. As a result, a cell count and cell size distribution like the one shown in Table B.2 is present, where some cells fall well below this target value. If left unattended, this cells would give unreasonable exchange terms (K_{sl}) as the the void fraction field (ϵ_s) would give completely unrealistic values. Thus, the general procedure is to use a divided void fraction model, like the one shown for regular materials in *LIGGGHTS*, where each particle is split into 29 equivolumetric regions and each sub-volume is assigned to the surrounding *CFD* cells resulting in a more accurate and smooth void fraction field. For superquadrics, a similar approach was used following the satellite point method [18] and assigning each point with the corresponding weight to the neighboring cells.

References

[1] J.L.V. Neto, C.R. Duarte, V.V. Murata, M.A.S. Barrozo, Effect of a draft tube on the fluid dynamics of a spouted bed: experimental and CFD studies, Drying Technol. 26 (3) (2008) 299–307.
[2] M.J. San José, S. Alvarez, A. Ortiz de Salazar, M. Olazar, J. Bilbao, Operating conditions of conical spouted beds with a draft tube. effect of the diameter of the draft tube and of the height of entrainment zone, Industr. Eng. Chem. Res. 46 (9) (2007) 2877–2884.
[3] A.G. Liden, F. Berruti, D.S. Scott, A kinetic model for the production of liquids from the flash pyrolysis of biomass, Chem. Eng. Commun. 65 (1) (1988) 207–221.
[4] G. Lopez, J. Alvarez, M. Amutio, B. Hooshdaran, M. Cortazar, M. Haghshenasfard, S.H. Hosseini, M. Olazar, Kinetic modeling and experimental validation of biomass fast pyrolysis in a conical spouted bed reactor, Chem. Eng. J. 373 (2019) 677–686.
[5] E. Rodríguez, A. Gutiérrez, R. Palos, F.J. Vela, J.M. Arandes, J. Bilbao, Fuel production by cracking of polyolefins pyrolysis waxes under fluid catalytic cracking (FCC) operating conditions, Waste Manage. 93 (2019) 162–172.
[6] A. Soria-Verdugo, M. Rubio-Rubio, E. Goos, U. Riedel, On the characteristic heating and pyrolysis time of thermally small biomass particles in a bubbling fluidized bed reactor, Renewable Energy 160 (2020) 312–322.
[7] M. Cortazar, G. Lopez, J. Alvarez, M. Amutio, J. Bilbao, M. Olazar, Behaviour of primary catalysts in the biomass steam gasification in a fountain confined spouted bed, Fuel 253 (2019) 1446–1456.
[8] Y. Gao, F.J. Muzzio, M.G. Ierapetritou, A review of the Residence Time Distribution (RTD) applications in solid unit operations 228 (2012) 416–423.
[9] L. Spreutels, J. Chaouki, F. Bertrand, B. Haut, R. Legros, Gas residence time distribution in a conical spouted bed, Powder Technol. 290 (2016) 62–71.
[10] M. Olazar, M.J. San José, F.J. Peñas, A.T. Aguyo, J.M. Arandes, J. Bilbao, "A model for gas flow in jet spouted beds," The, Can. J. Chem. Eng. 71 (2) (1993) 189–194.
[11] S. Pietsch, M. Schönherr, F. Kleine Jäger, S. Heinrich, Measurement of Residence Time Distributions in a Continuously Operated Spouted Bed, Chemical Engineering & Technology 43 (5) (2020) 804–812.
[12] I. Estiati, M. Tellabide, J. Saldarriaga, H. Altzibar, F. Freire, J. Freire, M. Olazar, Comparison of artificial neural networks with empirical correlations for estimating the average cycle time in conical spouted beds, Particuology 42 (2019) 48–57.
[13] P. Kieckhefen, S. Pietsch, M. Höfert, M. Schönherr, S. Heinrich, F. Kleine Jäger, Influence of gas inflow modelling on CFD-DEM simulations of three-dimensional prismatic spouted beds, Powder Technol. 329 (2018) 167–180.
[14] B. Hooshdaran, S. Hosseini, M. Haghshenasfard, M.N. Esfahany, M. Olazar, CFD modeling of heat transfer and hydrodynamics in a draft tube conical spouted bed reactor under pyrolysis conditions: Impact of wall boundary condition, Appl. Therm. Eng. 127 (2017) 224–232.
[15] F. Marchelli, C. Moliner, M. Curti, B. Bosio, E. Arato, CFD-DEM simulations of a continuous square-based spouted bed and evaluation of the solids residence time distribution, Powder Technol. 366 (2020) 840–858.
[16] F. Farivar, H. Zhang, Z. Tian, A. Gupte, CFD-DEM simulation of fluidization of multisphere- modelled cylindrical particles, Powder Technol. (2019).
[17] T. Al-Juwaya, N. Ali, M. Al-Dahhan, Investigation of cross-sectional gas-solid distributions in spouted beds using advanced non-invasive gamma-ray computed tomography (CT), Exp. Thermal Fluid Sci. 86 (sep 2017.) 37–53.
[18] X. Gao, J. Yu, L. Lu, C. Li, W.A. Rogers, Development and validation of superdem-cfd coupled model for simulating non-spherical particles hydrodynamics in fluidized beds, Chem. Eng. J. 420 (2021) 127654.
[19] S. Wang, Y. Shen, Super-quadric cfd-dem simulation of chip-like particles flow in a fluidized bed, Chem. Eng. Sci. 251 (2022) 117431.
[20] A. Atxutegi, P. Kieckhefen, S. Pietsch, R. Aguado, M. Olazar, S. Heinrich, Unresolved cfd-dem simulation of spherical and ellipsoidal particles in conical and prismatic spouted beds, Powder Technol. 389 (2021) 493–506.
[21] A.H. Barr, Superquadrics and Angle-Preserving Transformations, IEEE Comput. Graphics Appl. 1 (Jan 1981) 11–23.
[22] A. Podlozhnyuk, S. Pirker, C. Kloss, Efficient implementation of superquadric particles in Discrete Element Method within an open-source framework, Computational Particle Mechanics 4 (1) (2017) 101–118.
[23] X. Liu, J. Gan, W. Zhong, A. Yu, Particle shape effects on dynamic behaviors in a spouted bed: Cfd-dem study, Powder Technol. 361 (2020) 349–362.
[24] B. Mahmoodi, S.H. Hosseini, M. Olazar, H. Altzibar, CFD-DEM simulation of a conical spouted bed with open-sided draft tube containing fine particles, Journal of the Taiwan Institute of Chemical Engineers 81 (Dec 2017) 275–287.
[25] D. Feng, H. Li, M. Zhu, L. Han, Y. Zhou, Insight into the interaction mechanism between liquid action and cone structure in liquid-containing gas-solid spouted fluidized bed reactors, Powder Technol. 408 (2022) 117693.
[26] X. Wang, P. Kang, L. Cai, Y. Lu, J. Zhang, Z. Wang, Y. Zhou, Insight into multi-level fluidization characteristics of a spout-fluid bed under different gas-solid actions: From monodisperse particles to bidisperse particles, Powder Technol. 413 (2023) 118006.
[27] M. Tellabide, I. Estiati, A. Atxutegi, H. Altzibar, J. Bilbao, M. Olazar, Bed symmetry in the fountain confined conical spouted beds with open-sided draft tubes, Powder Technol. 399 (2022) 117011.
[28] H.C. Park, H.S. Choi, Visualization of flow structures inside a conical spouted bed by electrical capacitance volume tomography, Particuology 42 (2019) 15–25.
[29] M.J. San José, S. Alvarez, A. Morales, M. Olazar, J. Bilbao, Solid Cross-Flow into the Spout and Particle Trajectories in Conical Spouted Beds Consisting of Solids of Different Density and Shape, Chem. Eng. Res. Des. 84 (6) (2006) 487–494.
[30] M. Olazar, M.J. San José, R. Aguado, J. Bilbao, Solid Flow in Jet Spouted Beds, Industr. Eng. Chem. Res. 35 (8) (1996) 2716–2724.
[31] S.K. Sanjeevi, J.A. Kuipers, J.T. Padding, Drag, lift and torque correlations for non-spherical particles from Stokes limit to high Reynolds numbers, Int. J. Multiph. Flow 106 (2018) 325–337.
[32] F.R. Menter, M. Kuntz, R. Langtry, Ten Years of Industrial Experience with the SST Turbulence Model, in: in 4th Symposium on Turbulence Heat and Mass Transfer, Turbulence, heat and mass transfer, Begell House, (New York), 2003, pp. 625–632.
[33] N. Epstein, J.R. Grace, Spouted and spout-fluid beds: fundamentals and applications, Cambridge University Press, Cambridge, 2011.

[34] C. Goniva, C. Kloss, N.G. Deen, J.A. Kuipers, S. Pirker, Influence of rolling friction on single spout fluidized bed simulation, Particuology 10 (2012) 582–591, Oct.
[35] L. Spreutels, B., R. Legros, F. Bertrand, J. Chaouki, "Experimental investigation of solid particles flow in a conical spouted bed using radioactive particle tracking," AIChE J., vol. 62, no. 1, pp. 26–37, 2016.
[36] K. Chen, P. Bachmann, A. Bück, M. Jacob, E. Tsotsas, CFD simulation of particle residence time distribution in industrial scale horizontal fluidized bed, Powder Technol. 345 (2019) 129–139.
[37] S. Geng, Z. Han, J. Yue, Y. Li, X. Zeng, D. Lai, J. Yu, G. Xu, Conditioning micro fluidized bed for maximal approach of gas plug flow, Chem. Eng. J. 351 (2018) 110–118.
[38] H. Altzibar, I. Estiati, G. Lopez, J. Saldarriaga, R. Aguado, J. Bilbao, M. Olazar, Fountain confined conical spouted beds, Powder Technol. 312 (2017) 334–346.
[39] G.N.A. Vieira, F.B. Freire, J.T. Freire, Control of the moisture content of milk powder produced in a spouted bed dryer using a grey-box inferential controller, Drying Technol. 33 (15–16) (2015) 1920–1928.
[40] H. Altzibar, G. Lopez, I. Estiati, J. Bilbao, M. Olazar, Particle Cycle Times and Solid Circulation Rates in Conical Spouted Beds with Draft Tubes of Different Configuration, Industr. Eng. Chem. Res. 52 (45) (2013) 15959–15967.
[41] J.F. Saldarriaga, A. Atxutegi, R. Aguado, H. Altzibar, J. Bilbao, M. Olazar, Influence of contactor geometry and draft tube configuration on the cycle time distribution in sawdust conical spouted beds, Chem. Eng. Res. Des. 102 (2015) 80–89.
[42] M. Tellabide, I. Estiati, A. Pablos, H. Altzibar, R. Aguado, M. Olazar, New operation regimes in fountain confined conical spouted beds, Chem. Eng. Sci. 211 (2020).
[43] T. Lichtenegger, P. Kieckhefen, S. Heinrich, S. Pirker, Dynamics and long-time behavior of gas–solid flows on recurrent-transient backgrounds, Chem. Eng. J. 364 (2019) 562–577.